Dyes and Pigments 93 (2012) 1506–1511

Contents lists available at SciVerse ScienceDirect

Dyes and Pigments

journal homepage: www.elsevier.com/locate/dyepig

A comparative study of symmetrical and unsymmetrical trimethine cyanine dyes bearing benzoxazolyl and benzothiazolyl groups

Quan-Quan Shi [a], Ru Sun [a], Jian-Feng Ge [a,*], Qing-Feng Xu [b], Na-Jun Li [b], Jian-Mei Lu [a,b,*]

[a] Key Laboratory of Organic Synthesis of Jiangsu Province, Soochow University, Suzhou 215123, China
[b] Key Laboratory of Functional Materials for Environment Protection of Suzhou city, Soochow University, Suzhou 215123, China

ARTICLE INFO

Article history:
Received 29 July 2011
Received in revised form
7 November 2011
Accepted 7 November 2011
Available online 13 November 2011

Keywords:
Cyanine dye
Trimethine cyanine
Spectral property
DFT calculation
Benzoxazolyl
Benzothiazolyl

ABSTRACT

Six symmetrical and unsymmetrical trimethine cyanine dyes bearing benzothiazolyl and benzoxazolyl groups were synthesized. Their linear optical properties were studied. It was found that the variation of hetero atoms play an important role in the spectral properties of the dyes. Sequential replacement of the oxygen atom by the sulfur atom resulted in a change in shade from yellow to purple. In order to understand the relationship between the molecular structures and the spectral properties of these dyes, theoretical calculations were made using the Gaussian programme. Key parameters related to absorption and emission spectra were reported and discussed.

1. Introduction

Cyanine dyes have attracted interest as functional dyes in many fields. The extensively conjugated structures generate changeable absorption, high extinction coefficients and considerable quantum yields [1]. The applications of cyanine dyes and derivatives were mainly focused on the material and biological applications. In materials field, they may serve as non-linear optical (NLO) materials [2], data storage materials [3] and organic semiconductor materials [4]. In the biological arena, cyanine dyes have been used as probes for the detection of metal ions [5], DNA [6–8] and proteins [9]. In addition, their derivatives were also explored for anti-MRSA [10] and anti-protozoal [11] activity.

Much research on the spectral properties of cyanine dyes explored the influence of pH values [12], substituent groups [13], isomerism phenomenon [14] and the number of the methines. It is noted that benzothiazolyl and indolin-2-yl groups were the most common heterocyclic end groups in the studies of cyanine dyes. However, little research has explored the benzoxazolyl cyanine dyes [15]. In this study, the synthesis and comparative study of symmetrical and unsymmetrical trimethine cyanine dyes bearing benzoxazolyl and benzothiazolyl groups are discussed.

2. Experimental

2.1. General information

All the starting materials were purchased from either TCI or Sinopharm Chemical Reagent Co, Ltd. All analytic grade solvents (A.R.) were obtained from commercial suppliers and used directly. Melting points were determined on X-4 microscope electron thermal apparatus (Taike, China) without correction. Absorption spectra were taken on U-3900 UV–Vis spectrophotometer at room temperature. Fluorescence emission spectra were measured on Shimadzu RF-5300PC Spectroscope at room temperature. Quantum yields were determined using fluorescein in 0.1 M NaOH or cresyl violet in methanol as the reference. ^{1}H NMR spectra were recorded on either a Varian-300 or 400 NMR spectrometer, and TMS was used as an internal standard. Mass spectra were recorded on Finnigan MAT95 mass spectrometer (ESI$^+$). Elementary analysis was conducted on a Carlo Erba-MOD1106 elementary analysis apparatus. Differential scanning calorimetry (DSC) and thermogravimetric analysis (TGA) were conducted on a Universal V3.7A TA instrument in flowing N_2 with a heating rate of 10 °C/min.

* Corresponding authors. 199 Ren'ai Road, Suzhou Industrial Park, College of Chemistry, Chemical Engineering and Material Science, Soochow University, Suzhou 215123, China. Tel.: +86 (0) 512 6588 4717; fax: +86 (0) 512 6588 0367.
E-mail addresses: ge_jianfeng@hotmail.com (J.-F. Ge), lujm@suda.edu.cn (J.-M. Lu).

0143-7208/$ – see front matter © 2011 Elsevier Ltd. All rights reserved.
doi:10.1016/j.dyepig.2011.11.001

2.2. Synthesis

2.2.1. 2,3-Dimethylbenzoxazol-3-ium iodide (**1a**)

A solution of 2-methylbenzoxazole (2.66 g, 20.0 mmol) and iodomethane (11.28 g, 80.0 mmol) in DMF (10.0 mL) was heated at 60 °C for 24 h. The solution was cooled to room temperature, and then ethyl acetate (100.0 mL) was added slowly. The precipitated solid was collected by filtration and washed with ethyl acetate. The crude product was collected and heated under reflux with ethyl acetate (100.0 mL) for 15 min. The suspension was cooled to room temperature. The product was collected by filtration and washed with ethyl acetate to afford **1a** as bright yellow solid. Yield: 80.5%. ^{1}H NMR (400 MHz, DMSO-d_6, TMS) δ_H: 8.16–8.11 (m, 2H), 7.79–7.77 (m, 2H), 4.08 (s, 3H), 3.07 (s, 3H).

2.2.2. 2,3,5-Trimethylbenzoxazol-3-ium iodide (**1b**)

Compound **1b** was synthesized by the similar procedure of **1a**. Yield: 97.7%. ^{1}H NMR (400 MHz, DMSO-d_6, TMS) δ_H: 8.01 (d, J = 8.6 Hz, 1H), 7.93 (s, 1H), 7.59 (d, J = 8.6 Hz, 1H), 4.03 (s, 3H), 3.04 (s, 3H), 2.54 (s, 3H).

2.2.3. 2,3-Dimethylbenzothiazol-3-ium iodide (**1c**)

Compound **1c** was synthesized by the similar procedure of **1a**. Yield: 98.4%. ^{1}H NMR (400 MHz, DMSO-d_6, TMS) δ_H: 8.46 (d, J = 8.1 Hz, 1H), 8.30 (d, J = 8.5 Hz, 1H), 7.91–7.87 (m, 1H), 7.82–7.77 (m, 1H), 4.21 (s, 3H), 3.19 (s, 3H).

2.2.4. 2,3,5-Trimethylbenzothiazol-3-ium iodide (**1d**)

Compound **1d** was synthesized by the similar procedure of **1a**. Yield: 83.6%. ^{1}H NMR (400 MHz, DMSO-d_6, TMS) δ_H: 8.30 (d, J = 8.4 Hz, 1H), 8.14 (s, 1H), 7.64 (d, J = 8.4 Hz, 1H), 4.16 (s, 3H), 3.15 (s, 3H), 2.57 (s, 3H).

2.2.5. 3-Methyl-2-(2-(N-phenylacetamido)vinyl)benzoxazol-3-ium iodide (**2a**)

A suspension of **1a** (1.58 g, 5.7 mmol) and N, N′-diphenylformamidine (1.36 g, 6.9 mmol) in acetic anhydride (10.0 mL) was heated under reflux for 2 h. The reaction was cooled to room temperature; ethyl ether (30.0 mL) was added slowly over more than 0.5 h. The product was collected by filtration, then washed with ethyl ether (3 × 15.0 mL) and water (3 × 5.0 mL) to afford **2a** as a yellow solid. Yield: 46.1%. mp. 173–174 °C ^{1}H NMR (400 MHz, DMSO-d_6, TMS) δ_H: 9.06 (d, J = 13.8 Hz, 1H), 8.06 (d, J = 7.4 Hz, 1H), 7.94 (d, J = 7.4 Hz, 1H), 7.69–7.65 (m, 5H), 7.53 (d, J = 7.5 Hz, 2H), 5.46 (d, J = 13.7 Hz, 1H), 3.80 (s, 3H), 2.06 (s, 3H). ESI$^+$ m/z: calcd for $C_{18}H_{17}N_2O_2^+$: 293.1285, found: 293.1276.

2.2.6. 3-Methyl-2-(3-(3-methylbenzoxazol-2(3H)-ylidene)prop-1-en-1-yl)benzoxazol-3-ium chloride (**3a**)

To a solution of **1a** (3.56 g, 13.0 mmol) in acetic anhydride (10.0 mL) under reflux, triethoxymethane (1.92 g, 13.0 mmol) was added dropwise during 45 min under nitrogen. The reaction was heated under reflux for 1 h. After it was cooled to room temperature, the residue was collected by filtration, washed by ethyl acetate (3 × 15.0 mL) and water (3 × 15.0 mL). The iodide salt was obtained by recrystallization in ethanol. Then the iodide salt was dissolved in methanol. The methanol solution was passed through the anion-exchange resin (Amberlite IRA-400, chloride form), and the resin was washed with methanol. After the concentration of the eluent chloride salt, the product was collected to give **3a** as red solid. Yield: 8.7%. mp. 214.6–215.0 °C ^{1}H NMR (300 MHz, DMSO-d_6, TMS) δ_H: 8.29 (t, J = 13.7 Hz, 1H), 7.76 (d, J = 7.5 Hz, 2H), 7.67 (d, J = 7.3 Hz, 2H), 7.53–7.33(m, 4H), 6.03 (d, J = 13.2 Hz, 2H), 3.74 (s, 6H). ESI$^+$ m/z: calcd for $C_{19}H_{17}N_2O_2^+$: 305.1285, found: 305.1285. Anal. Calcd. for $C_{19}H_{17}ClN_2O_2\cdot 2.5H_2O$: C, 59.14; H, 5.75; N, 7.26. found: C, 58.87; H, 5.55; N, 7.20.

2.2.7. 3-Methyl-2-(3-(3-methylbenzothiazol-2(3H)-ylidene)prop-1-en-1-yl)benzoxazol-3-ium chloride (**3b**)

To a mixture of **2a** (0.10 g, 0.25 mmol) and **1c** (0.072 g, 0.25 mmol) in ethanol (6 mL), Et_3N (0.1 mL) was added in portions, and then the mixture was heated under reflux for 1 h. The reaction was cooled to room temperature; ethyl ether (10 mL) was added slowly during 0.5 h. The solid was filtrated, washed with ethyl ether (3 × 10.0 mL) and water (3 × 10.0 mL) to afford the iodide salt. Then the iodide salt was dissolved in methanol. The methanol solution of the iodide salt was passed through the anion-exchange resin (Amberlite IRA-400, chloride form), and the resin was washed with methanol. After the concentration of the eluent chloride salt, the product was collected to give **3b** as dark red solid. Yield: 59.1%. mp.210.0–210.9 °C ^{1}H NMR (300 MHz, DMSO-d_6, TMS) δ_H: 8.05–7.93 (m, 2H), 7.81–7.65 (m, 3H), 7.60–7.35 (m, 4H), 6.50 (d, J = 12.4 Hz, 1H), 6.08 (d, J = 12.8 Hz, 1H), 3.82 (s, 3H), 3.74 (s, 3H). ESI$^+$ m/z: calcd for $C_{19}H_{17}N_2OS^+$: 321.1056, found: 321.1061. Anal. Calcd. for $C_{19}H_{17}ClN_2OS\cdot 4H_2O$: C, 53.20; H, 5.87; N, 6.53. found: C, 53.37; H, 5.45; N, 6.54.

2.2.8. 3-Methyl-2-(3-(3-methylbenzothiazol-2(3H)-ylidene)prop-1-en-1-yl)benzothiazol-3-ium chloride(**3c**)

Dye **3c** was synthesized by condensing **1c** and triethoxymethane by a similar procedure described for dye **3a**. Yield: 41.7%. mp. 217.0–218.0 °C ^{1}H NMR (300 MHz, DMSO-d_6, TMS) δ_H: 7.99 (d, J = 7.7 Hz, 2H), 7.78–7.66 (m, 3H), 7.56 (t, J = 7.5 Hz, 2H), 7.39 (t, J = 7.4 Hz, 2H), 6.54 (d, J = 12.5 Hz, 2H), 3.82 (s, 6H). ESI$^+$ m/z: calcd for $C_{19}H_{17}N_2S_2^+$: 337.0828, found: 337.0821. Anal. Calcd. for $C_{19}H_{17}ClN_2S_2\cdot 4H_2O$: C, 51.28; H, 5.66; N, 6.30. found: C, 50.94; H, 5.20; N, 6.25.

2.2.9. 2-(3-(3,5-Dimethylbenzoxazol-2(3H)-ylidene)prop-1-en-1-yl)-3-methylbenzoxazol-3-ium chloride (**3d**)

Dye **3d** was synthesized by condensing **2a** and **1b** by a similar procedure described for dye **3b**. Yield: 38.1%. mp. 213.9–214.1 °C ^{1}H NMR (300 MHz, DMSO-d_6, TMS) δ_H: 8.25 (t, J = 13.1 Hz, 1H), 7.74 (d, J = 6.9 Hz, 1H), 7.65–7.61 (m, 2H), 7.54–7.35 (m, 3H), 7.20 (d, J = 7.2 Hz, 1H), 6.10–5.92 (m, 2H), 3.71 (s, 6H), 2.43 (s, 3H). ESI$^+$ m/z: calcd for $C_{20}H_{19}N_2O_2^+$: 319.1447, found: 319.1436. Anal. Calcd. for $C_{20}H_{19}ClN_2O_2\cdot 2.5H_2O$: C, 60.07; H, 6.05; N, 7.01. found: C, 60.24; H, 5.56; N, 6.98.

2.2.10. 2-(3-(3,5-Dimethylbenzothiazol-2(3H)-ylidene)prop-1-en-1-yl)-3-methylbenzoxazol-3-ium chloride (**3e**)

Dye **3e** was synthesized by condensing **2a** and **1d** by a similar procedure described for dye **3b**. Yield: 91.7%. mp. 203.7–204.1 °C ^{1}H NMR (300 MHz, DMSO-d_6, TMS) δ_H: 8.05–7.89 (m, 1H), 7.83 (d, J = 7.5 Hz, 1H), 7.76–7.72 (m, 1H), 7.67–7.65 (m, 1H), 7.58 (s, 1H), 7.52–7.33 (m, 2H), 7.22–7.20 (m, 1H), 6.49 (d, J = 12.7 Hz, 1H), 6.03 (d, J = 13.0 Hz, 1H), 3.80 (s, 3H), 3.72 (s, 3H), 2.43 (s, 3H). ESI$^+$ m/z: calcd for $C_{20}H_{19}N_2OS^+$: 335.1218, found: 335.1212. Anal. Calcd. for $C_{20}H_{19}ClN_2OS\cdot 4H_2O$: C, 54.23; H, 6.14; N, 6.32. found: C, 53.79; H, 5.68; N, 6.08.

2.2.11. 2-(3-(3,5-Dimethylbenzothiazol-2(3H)-ylidene)prop-1-en-1-yl)-3-methylbenzothiazol-3-ium chloride (**3f**)

Dye **3f** was synthesized by condensing **2c** and **1d** by a similar procedure described for dye **3b**. Yield: 72.3%. mp. 210.7–211.2 °C ^{1}H NMR (300 MHz, DMSO-d_6, TMS) δ_H: 7.97 (d, J = 7.6 Hz, 1H), 7.85 (d, J = 7.8 Hz, 1H), 7.75–7.67 (m, 2H), 7.58–7.53 (m, 2H), 7.39 (t, J = 7.4 Hz, 1H), 7.22 (d, J = 7.9 Hz, 1H), 6.51 (t, J = 11.0 Hz, 2H), 3.80 (s, 6H), 2.43 (s, 3H). ESI$^+$ m/z: calcd for $C_{20}H_{19}N_2S_2^+$: 351.0990,

found: 351.0977. Anal. Calcd. for $C_{20}H_{19}ClN_2S_2 \cdot 2.5H_2O$: C, 54.47; H, 5.71; N, 6.35. found: C, 54.99; H, 5.42; N, 6.23.

3. Results and discussion

3.1. Synthesis

The synthetic strategy used to obtain the dyes **3a**–**f** was shown in Scheme 1. Compounds **1a**–**d** were prepared by the reaction of the requisite starting material and iodomethane in DMF at 60 °C [16–18]. The intermediates **2a** and **2c** were synthesized in the similar way described in references [19,20] with some modifications. The symmetrical cyanine dyes (**3a**, **3c**) were obtained by the condensation of **1a** and **1c** with triethoxymethane in acetic anhydride, respectively. The unsymmetrical cyanines were obtained by the reaction of compounds **1** and **2**, which followed the last step in the preparation of rhodacyanine [11]. To improve the solubility of the final products, the chloride salts were obtained from the corresponding iodide salts using ion-exchange technology. The TGA analyses were shown in Fig. S1 (Supplementary data). The molecules of water of crystallization associated with the dyes were lost during heating between 50 and 150 °C and the dyes were decomposed around 250 °C.

3.2. Spectral properties of dyes *3a–f*

UV–vis and fluorescence spectra of dyes **3a**–**f** in DMSO solution are presented in Figs. 1 and 2, respectively. The spectral characteristics including absorption and emission maxima (λ_{max}), excitation wavelength (λ_{ex}), extinction coefficients (ε), Stokes' shift ($\Delta\nu_{st}$) and fluorescence quantum yields (Φ) are given in Table 1.

As shown in Fig. 1, the absorption spectra of dyes **3a**–**f** show typical absorption bands of cyanine dyes: an intense dominant absorption band with one shoulder band. Comparing **3a**, **3b** with **3c**, the maximum absorption bands gradually increase (**3a** < **3b** < **3c**). The same situation is also found in **3d**, **3e** and **3f** (**3d** < **3e** < **3f**). The results indicate that the hetero atoms play an important role in the absorption spectra. There is a 20 nm red-shift with the variation of the hetero atoms from oxygen to sulfur. The methyl group on the benzene ring induces a slight red-shift (about 3 nm). The fluorescence spectra of dyes **3a**-**f** display the same phenomenon. The

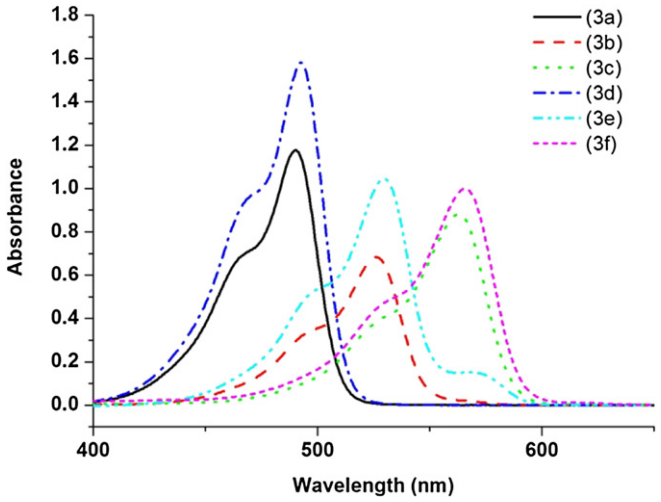

Fig. 1. UV/visible absorption spectra of dyes **3a**–**f** at the concentration of 1.0×10^{-5} mol L^{-1} In DMSO solution.

Stokes' Shifts of these dyes are 20–22 nm. Dyes **3a** and **3d** possess moderate quantum yields (0.35, 0.34), comparing with dyes **3c** (0.15) and **3f** (0.17).

3.3. Theoretical calculations

3.3.1. Computational details

All the calculations in this work were performed with the Gaussian98 program package [21]. The geometric and electronic structures of molecules were investigated with the DFT method. In each optimization, the vibrational frequencies were calculated and the results showed that all optimized structures were stable geometric structures. The lowest singlet excited states were computed with *ab initio* CIS/6-31G(d) on the basis of the optimized geometries obtained from HF/6-31G(d) calculations. The transition energies were calculated at the ground-state and excited-state geometries using TD-DFT calculations. The maximum absorption and emission wavelengths of these compounds were studied by employing TD-DFT methods. The transition energies were

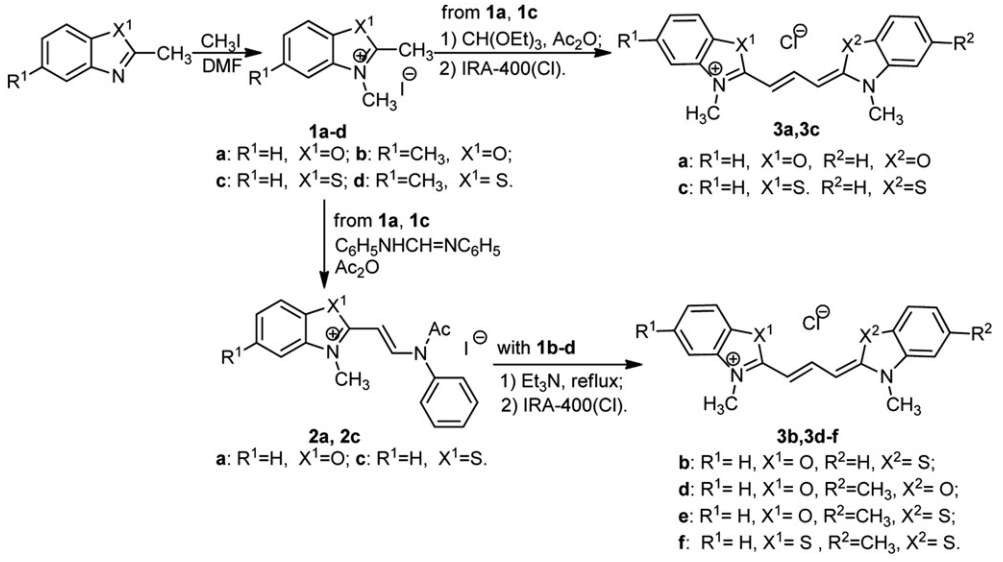

Scheme 1. The synthetic route to dyes **3a**–**f**.

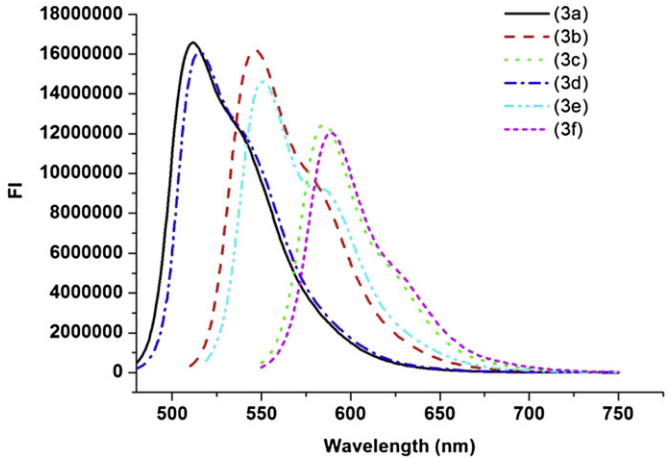

Fig. 2. Fluorescence emission spectra of dyes **3a**–**f** at the concentration of 1.0×10^{-5} mol L^{-1} in DMSO solution.

calculated at the TD-DFT/B3LYP level of approximation by using the ground (excited) state HF/6-31G(d) (CIS/6-31G(d)) geometries, which are considered to precisely predict the absorption and fluorescence spectra of these systems [22–25]. The polarizable continuum model (PCM) was used in calculation of the absorption and emission spectra in DMSO solution. The singlet–triplet gaps were calculated at the optimized geometry of the first excited singlet. All DFT calculations were performed using the B3LYP functional and the 6-31G (d) basis set.

3.3.2. Geometry optimization and NBO charge distribution

Some selected bond lengths, bond angles and dihedral angles are shown in Table 2. The optimized structures of the cation parts for dyes **3a**–**f** at the ground state are represented in Fig. S2 (Supplementary data). As shown in Table 2, the bond angles of C–S–C are in the range from 89.35° to 89.58°, however, the bond angles of C–O–C are from 107.36° to 107.43°. The bond lengths of C–S are in the range from 1.817 Å to 1.825 Å, while the bond lengths of C–O are from 1.383 Å to 1.417 Å. The calculated bond lengths and bond angles suggest that the hetero atoms have a great influence on the molecular structures of dyes **3a-f**. From Table 2 and the optimized structures of dyes $\mathbf{3a}^+$–$\mathbf{f}^+$ (supplementary data), it can be seen that dyes $\mathbf{3a}^+$–$\mathbf{f}^+$ are π-conjugated planar compounds. The dihedral angles of C_1–C_2–O–C_4, C_1–C_2–S–C_4, C_5–C_4–O–C_2 and C_5–C_4–S–C_2 are in the range from 179.02° to 179.96°, which indicate that the hetero atoms do not distort the planarity.

The NBO charge distributions are shown in Table 3, from these data, it can be seen that the NBO charges of the sulfur atoms are in the range from 0.411 to 0.414, while the NBO charges of the oxygen atoms are from −0.461 to −0.416. The charges of carbon atoms connected to sulfur atoms are from −0.193 to 0.126. However, the charges are from 0.283 to 0.612 when they connected to oxygen atoms. Compared with the oxygen atom the sulfur atom has a stronger electronic donation ability.

3.3.3. Absorption spectra

The key parameters related to absorption spectra are listed in Table 4. As shown in Table 4, the excitation energies from dyes $\mathbf{3a}^+$ to $\mathbf{3c}^+$ and from dyes $\mathbf{3d}^+$ to $\mathbf{3f}^+$ decrease, meanwhile, the maximum absorption bands increase. The dominant transitions of dyes $\mathbf{3a}^+$–$\mathbf{f}^+$ are HOMO to LUMO transitions (Table S1, supplementary data). The frontier molecular orbitals of $\mathbf{3a}^+$–$\mathbf{f}^+$ are shown in Fig. S3 (supplementary data), it can be seen that the HOMO of dyes $\mathbf{3a}^+$–$\mathbf{f}^+$ are mainly located on the hetero rings and the carbon atoms connected to the hetero rings. Compared with an oxygen atom, the sulfur atom has a noticeable contribution to its HOMO component. Meanwhile the LUMO are mainly located on the methine chain and the sulfur atom also has a discernible contribution to its LUMO

Table 1
Absorption and emission maxima (λ_{max}), excitation wavelength (λ_{ex}), extinction coefficients (ε), Stokes' shift ($\Delta\nu_{st}$) and quantum yields (Φ) of dyes **3a**–**f**.

Dyes	λ_{max}(Abs) (nm)	λ_{max}(Em)[a] (nm)	lg ε (L mol^{-1} cm^{-1})	$\Delta\nu_{st}$ (nm)	Φ
3a	490	512	5.06	22	0.35[b]
3b	526	546	4.84	20	0.26[b]
3c	563	585	4.95	22	0.15[c]
3d	493	515	5.20	22	0.34[b]
3e	530	551	5.02	21	0.20[b]
3f	566	588	5.00	22	0.17[c]

[a] The results were obtained by the excitation on the absorption maximum.
[b] The fluorescence quantum yields (Φ) were measured in DMSO solution using fluorescein in 0.1 mol L^{-1}NaOH as the reference.
[c] The fluorescence quantum yields (Φ) were measured in DMSO solution using cresyl violet in methanol as the reference.

Table 2
Selected bond lengths (R, Å), bond angles (D, °) and dihedral angles (Di, °) of $\mathbf{3a}^+$–$\mathbf{f}^+$.

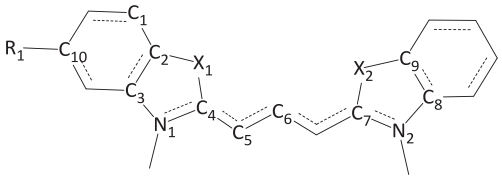

	$\mathbf{3a}^+$	$\mathbf{3b}^{+a}$	$\mathbf{3c}^+$	$\mathbf{3d}^+$	$\mathbf{3e}^+$	$\mathbf{3f}^+$
R(C_1–C_2)	1.381	1.390	1.390	1.382	1.388	1.391
R(C_2–X_1)	1.417	1.825	1.824	1.417	1.823	1.823
R(C_4–X_1)	1.384	1.818	1.818	1.383	1.822	1.817
R(C_4–C_5)	1.391	1.397	1.397	1.392	1.399	1.398
R(C_4–N_1)	1.367	1.366	1.366	1.367	1.366	1.365
R(C_3–N_1)	1.414	1.416	1.416	1.415	1.415	1.417
R(C_7–X_2)	–	1.384	–	1.385	1.385	1.818
R(C_9–X_2)	–	1.416	–	1.416	1.417	1.824
R(C_7–N_2)	–	1.367	–	1.367	1.367	1.366
R(R_1–C_{10})	–	–	–	1.512	1.513	1.511
D(C_2–X_1–C_4)	107.40	89.38	89.39	107.36	89.58	89.35
D(C_3–N_1–C_4)	109.16	115.90	115.89	109.15	115.93	115.88
D(C_7–X_2–C_9)	–	107.43	–	107.40	107.38	89.38
D(C_7–N_2–C_8)	–	109.16	–	109.17	109.17	115.91
Di(C_1–C_2–X_1–C_4)	179.96	179.68	179.75	179.91	179.88	179.69
Di(C_5–C_4–X_1–C_2)	179.70	179.02	179.17	179.35	179.19	179.04

[a] For $\mathbf{3b}^+$, X_1 is sulfur atom.

Table 3
NBO charge distribution of $\mathbf{3a}^+$–$\mathbf{f}^+$.

	$\mathbf{3a}^+$	$\mathbf{3b}^{+a}$	$\mathbf{3c}^+$	$\mathbf{3d}^+$	$\mathbf{3e}^+$	$\mathbf{3f}^+$
C_1	−0.256	−0.227	−0.227	−0.252	−0.221	−0.221
C_2	0.291	−0.187	−0.186	0.283	−0.193	−0.193
C_3	0.115	0.143	0.143	0.121	0.150	−0.150
C_4	0.611	0.126	0.125	0.612	0.125	0.122
C_5	−0.404	−0.375	−0.368	−0.404	−0.374	−0.367
C_6	−0.102	−0.107	−0.112	−0.104	−0.109	−0.114
C_7	–	0.609	–	0.610	0.609	0.122
C_8	–	0.115	–	0.115	0.115	0.144
C_9	–	0.290	–	0.289	0.290	−0.186
C_{10}	–	–	–	−0.008	−0.002	−0.001
N_1	−0.390	−0.364	−0.362	−0.382	−0.363	−0.362
N_2	–	−0.381	–	−0.384	−0.383	−0.364
X_1	−0.461	0.412	0.411	−0.458	0.414	0.414
X_2	–	−0.459	–	−0.460	−0.416	0.412

[a] For $\mathbf{3b}^+$, X_1 is sulfur atom.

Table 4
Absorption spectra were obtained using TD-DFT methods for dyes $\mathbf{3a}^+$–$\mathbf{f}^+$ at the B3LYP/6-31G(d) Optimized Geometries.

		electronic transitions	exp[a] (nm)	λ_{max}^{abs} (nm)	*f*	excitation energies (eV)
$\mathbf{3a}^+$	gas phase	S0 → S1		409	1.57	3.02
	DMSO	S0 → S1	490	434	1.75	2.85
$\mathbf{3b}^+$	gas phase	S0 → S1		431	1.47	2.87
	DMSO	S0 → S1	526	458	1.66	2.70
$\mathbf{3c}^+$	gas phase	S0 → S1		455	1.39	2.72
	DMSO	S0 → S1	563	485	1.58	2.55
$\mathbf{3d}^+$	gas phase	S0 → S1		409	1.58	3.02
	DMSO	S0 → S1	493	435	1.79	2.84
$\mathbf{3e}^+$	gas phase	S0 → S1		435	1.48	2.84
	DMSO	S0 → S1	530	461	1.64	2.69
$\mathbf{3f}^+$	gas phase	S0 → S1		460	1.40	2.69
	DMSO	S0 → S1	566	488	1.59	2.53

[a] Measured in DMSO solution.

component. The simulated absorption spectrum in the gas phase and in DMSO solution is shown in Fig. S4 (supplementary data). The simulated results correlate closely with the experimental results.

3.3.4. Emission spectra

The key parameters related to fluorescence emission spectra are listed in Table 5. From Table 5, it can be seen that the trend of the calculated emission spectra data fits that of the experimental results, although there are discrepancies between theoretical values and experimental values. There are several reasons for the discrepancies. Firstly, the currently available calculated methods are approximate methods; the improved methods are still under development. Secondly, the treatment of the solvent is also a limitation and calculations of the specific interactions with solvent molecules are not taken into account. As many researchers have reported [26,27], solvent has a great influence on the fluorescence emission spectra.

The results show that the fluorescence quantum yields decrease from dyes **3a** to **3c** and from **3d** to **3f** (Table 1). The possible explanation is a low singlet–triplet gap, which increases the probability of the non-radiative processes and a strong spin–orbit coupling, duing to the presence of the sulfur atom in the π-electronic system. According to the literature [28], the sulfur atom in an aromatic system such as dibenzothiophene increases the ratio of phosphorescence/fluorescence quantum yields, due to spin–orbit coupling and electronic effects. The calculated values for the singlet–triplet splitting are listed in Table 6. A decrease of singlet–triplet gap is found from $\mathbf{3a}^+$ to $\mathbf{3c}^+$ and $\mathbf{3d}^+$ to $\mathbf{3f}^+$. The calculated results in Table 6 predict a higher probability of the intersystem crossing (ISC) processes and increase the rate of the overall non-radiative processes, which are in agreement with the experimental results.

Table 5
Calculated Emission Data in the gas phase and in DMSO solution for dyes $\mathbf{3a}^+$–$\mathbf{f}^+$.

		electronic transitions	exp[a] (nm)	λ_{max}^{em} (nm)	*f*	excitation energies (eV)
$\mathbf{3a}^+$	gas phase	S1 → S0		411	1.58	3.01
	DMSO	S1 → S0	512	436	1.75	2.84
$\mathbf{3b}^+$	gas phase	S1 → S0		436	1.46	2.84
	DMSO	S1 → S0	546	466	1.64	2.66
$\mathbf{3c}^+$	gas phase	S1 → S0		461	1.40	2.68
	DMSO	S1 → S0	585	493	1.57	2.51
$\mathbf{3d}^+$	gas phase	S1 → S0		416	1.60	2.97
	DMSO	S1 → S0	515	439	1.77	2.82
$\mathbf{3e}^+$	gas phase	S1 → S0		443	1.43	2.79
	DMSO	S1 → S0	551	468	1.63	2.64
$\mathbf{3f}^+$	gas phase	S1 → S0		467	1.40	2.65
	DMSO	S1 → S0	588	497	1.58	2.49

[a] Measured in DMSO solution.

Table 6
Singlet–triplet gaps of $\mathbf{3a}^+$–$\mathbf{f}^+$ (ΔE_{ST}).

		$\mathbf{3a}^+$	$\mathbf{3b}^+$	$\mathbf{3c}^+$	$\mathbf{3d}^+$	$\mathbf{3e}^+$	$\mathbf{3f}^+$
ΔE_{ST} (cm^{-1})	Gas phase	9347	9239	9142	9177	9056	8994
	DMSO	7907	7817	7687	7822	7728	7615

4. Conclusion

Six symmetrical and unsymmetrical trimethine cyanine dyes **3a**–**f** were synthesized. Their linear optical properties were investigated experimentally and theoretically. The experimental results showed that their absorption bands and fluorescence bands were shifted by about 20 nm when one oxygen atom was replaced by one sulfur atom. The NBO charge distribution indicated that the sulfur atoms possess stronger electronic donation ability. Theoretical results showed that their excited energies decrease in the order **3a**, **3b** to **3c** and **3d**, **3e** to **3f**. The reason for the lower excited energies is the presence of lower lying unoccupied states in the case of the sulfur atoms, in comparison to oxygen atoms. All the dominant transitions are HOMO to LUMO transitions, and the maximum absorption bands shift both in the gas phase and in DMSO solution. The simulated spectra results correlate closely with the experimental results.

Acknowledgments

We thank the financial support from National Natural Science Foundation of China (20876101, 21071105, 20902065), Natural Science Fund (BK2009113) in Jiangsu Province.

Appendix. Supplementary material

Supplementary material associated with this article can be found, in the online version, at doi:10.1016/j.dyepig.2011.11.001.

References

[1] Peng X, Song F, Lu E, Wang Y, Zhou W, Fan J, et al. Heptamethine cyanine dyes with a large stokes shift and strong fluorescence: a paradigm for excited-state intramolecular charge transfer. J Am Chem Soc 2005;127:4170–1.
[2] Hales JM, Matichak J, Barlow S, Ohira S, Yesudas K, Brédas J-L, et al. Design of polymethine dyes with large third-order optical nonlinearities and loss figures of merit. Science 2010;327:1485–8.
[3] Mustroph H, Stollenwerk M, Bressau V. Current developments in optical data storage with organic dyes. Angew Chem Int Edn 2006;45:2016–35.
[4] Spitler MT, Parkinson BA. Dye sensitization of single crystal semiconductor electrodes. Acc Chem Res 2009;42:2017–29.
[5] Nolan EM, Lippard SJ. Tools and tactics for the optical detection of mercuric ion. Chem Rev 2008;108:3443–80.
[6] Levitus M, Ranjit S. Cyanine dyes in biophysical research: the photophysics of polymethine fluorescent dyes in biomolecular environments. Q Rev Biophys 2011;44:123–51.
[7] Flors C. DNA and chromatin imaging with super-resolution fluorescence microscopy based on single-molecule localization. Biopolymers 2011;95:290–7.
[8] Hannah KC, Armitage BA. DNA-templated assembly of helical cyanine dye aggregates: A supramolecular chain polymerization. Acc Chem Res 2004;37:845–53.
[9] Volkova KD, Kovalska VB, Balanda AO, Vermeij RJ, Subramaniam V, Slominskii YL, et al. Cyanine dye-protein interactions: looking for fluorescent probes for amyloid structures. J Biochem Bioph Meth 2007;70:727–33.
[10] Wainwright M, Kristiansen JE. Quinoline and cyanine dyes – putative anti-MRSA drugs. Int J Antimicrob Ag 2003;22:479–86.
[11] Yang M, Arai C, Bakar Md A, Lu J, Ge J-F, Pudhom K, et al. Fluorinated rhodacyanine (SLJ-01) possessing high efficacy for visceral leishmaniasis (VL). J Med Chem 2010;53:368–73.

[12] Mazières MR, Duprat C, Wolf JG, Roshal AD. Ph dependent spectral properties and electronic structure of benzothiazol containing cyanine dyes. Dyes Pigm 2009;80:355–60.
[13] Mitekura H, No T, Suzuki K, Satake K, Kimura M. Spectroscopic properties of meso-substituted cyanine dyes: evidences for intramolecular charge transfer from a julolidine moiety as a meso-substituent to the cyanine chromophore. Dyes Pigm 2002;54:113–20.
[14] West W, Pearce S, Grum F. Stereoisomerism in cyanine dyes – meso-substituted thiacarbocyanines. J Phys Chem 1967;71:1316–26.
[15] Mishra A, Behera R, Behera P, Mishra B, Behera G. Cyanines during the 1990s: a review. Chem Rev 2000;100:1973–2012.
[16] Deligeorgiev T, Kaloyanova S, Vasilev A. A novel general method for preparation of neutral monomethine cyanine dyes. Dyes Pigm 2011;90:170–6.
[17] Kabatc J, Paczkowski J. The photophysical and photochemical properties of the oxacarbocyanine and thiacarbocyanine dyes. Dyes Pigm 2004;61:1–16.
[18] Peng Z-H, Zhou X-F, Carroll S, Geise HJ, Peng B-x, Dommisse R, et al. Structure of rhodanine cyanine dyes, spectroscopy and performance in photographic emulsions. J Mater Chem 1996;6:1325–33.
[19] Carreon JR, Stewart KM, Mahon Jr KP, Shin S, Kelley SO. Cyanine dye conjugates as probes for live cell imaging. Bioorg Med Chem Lett 2007;17:5182–5.
[20] Jung ME, Kim W-J. Practical syntheses of dyes for difference gel electrophoresis. Bioorgan Med Chem 2006;14:92–7.
[21] Frisch MJ, Trucks GW, Schlegel HB, Scuseria GE, Robb MA, Cheeseman JR, et al. Gaussian 98 revision A.5. Pittsburgh, PA: Gaussian, Inc.; 2003.
[22] Zhang X-H, Wang L-Y, Zhai G-H, Wen Z-Y, Zhang Z-X. The absorption, emission spectra as well as ground and excited states calculations of some dimethine cyanine dyes. J Mol Struc THEOCHEM 2009;906:50–5.
[23] Meguellati K, Ladame S, Spichty M. A conceptually improved TD-DFT approach for predicting the maximum absorption wavelength of cyanine dyes. Dyes Pigm 2011;90:114–8.
[24] Champagne B, Guillaume M, Zutterman F. TDDFT investigation of the optical properties of cyanine dyes. Chem Phys Lett 2006;425:105–9.
[25] Guillaume M, Liégeois V, Champagne B, Zutterman F. Time-dependent density functional theory investigation of the absorption and emission spectra of a cyanine dye. Chem Phys Lett 2007;446:165–9.
[26] Tomasi J, Mennucci B, Cammi R. Quantum mechanical continuum solvation models. Chem Rev 2005;105:2999–3094.
[27] Fdez Galván I, Elena Martín M, Muñoz-Losa A, Aguilar MA. Solvatochromic shifts on absorption and fluorescence bands of N, N-dimethylaniline. J Chem Theory Comput 2009;5:341–9.
[28] Ionescu S, Popovici D, Balaban AT, Hillebrand M. 2-phenoxathiinyl-5-phenyloxazole and 5-phenoxathiinyl-2-phenyloxazole derivatives: experimental and theoretical study of emission properties. Spectrochim Acta A 2007;66:1165–70.